Non-Intrusive Load Monitoring Under Residential Solar Power Influx

Chinthaka Dinesh[a,b,*], Shirantha Welikala[a], Yasitha Liyanage[a], Mervyn Parakrama B. Ekanayake[a], Roshan Indika Godaliyadda[a], Janaka Ekanayake[a,c]

[a] *Department of Electrical and Electronic Engineering, Faculty of Engineering, University of Peradeniya, Sri Lanka.*
[b] *School Of Engineering Science, Simon Fraser University, Canada.*
[c] *School of Engineering, Cardiff University, United Kingdom.*

Abstract

This paper proposes a novel Non-Intrusive Load Monitoring (NILM) method for a consumer premises with a residentially installed solar plant. This method simultaneously identifies the amount of solar power influx as well as the turned ON appliances, their operating modes, and power consumption levels. Further, it works effectively with a single active power measurement taken at the total power entry point with a sampling rate of 1 Hz. First, a unique set of appliance and solar signatures were constructed using a high-resolution implementation of Karhunen Loéve expansion (KLE). Then, different operating modes of multi-state appliances were automatically classified utilizing a spectral clustering based method. Finally, using the total power demand profile, through a subspace component power level matching algorithm, the turned ON appliances along with their operating modes and power levels as well as the solar influx amount were found at each time point. The proposed NILM method was first successfully validated on six synthetically generated houses (with solar units) using real household data taken from the Reference Energy Disaggregation Dataset (REDD) - USA. Then, in order to demonstrate the scalability of the proposed NILM method, it was employed on a set of 400 individual households. From that, reliable estimations were obtained for the total residential solar generation and for the total load that can be shed to provide reserve services. Finally, through a developed prediction technique, NILM results observed from 400 households during four days in the recent past were utilized to predict the next day's total load that can be shed.

*Corresponding Author

Email addresses: hchintha@sfu.ca; dineshhgcp@gmail.com (Chinthaka Dinesh), shirantha.welikala.2015@IEEE.org; shirantha27@gmail.com (Shirantha Welikala), yasithashehanliyanage@gmail.com; wlysliyanage@IEEE.org (Yasitha Liyanage), mpb.ekanayake@ee.pdn.ac.lk (Mervyn Parakrama B. Ekanayake), roshangodd@ee.pdn.ac.lk (Roshan Indika Godaliyadda), jbe@ee.pdn.ac.lk; EkanayakeJ@cardiff.ac.uk (Janaka Ekanayake)

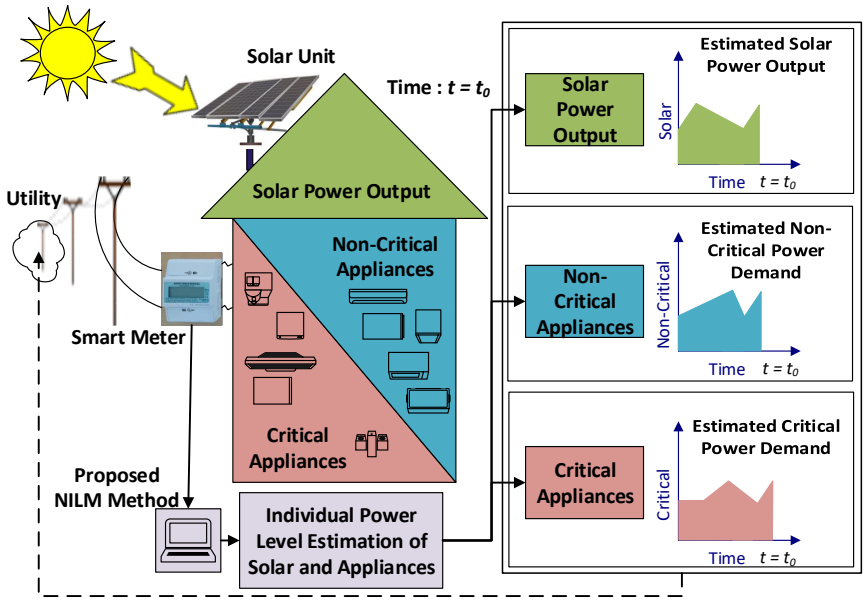

Figure 1: Graphical Abstract

Keywords: Non-Intrusive Load Monitoring (NILM), Operating Mode Estimation, Solar Power Estimation, Demand Response (DR), Demand Side Management (DSM), Smart Grid.
2010 MSC: 00-02, 62P30, 68P30, 99-00

Nomenclature: Acronyms & Symbols

Acronyms:

ACM	Autocorrelation Matrix
CV	Continuously Varying
CS	Cooking Stove
DR	Demand Response
DSM	Demand Side Management
DLC	Direct Load Control
DW	Dish Washer
FN	False Negatives
FP	False Positives
FES	First Elimination Step
KLE	Karhunen Loéve expansion
LHV	Likelihood Value
LM1	Lamp 1: 60W
LM2	Lamp 2: 100W
MAE	Mean Absolute Error
MAPE	Mean Absolute Percentage Error
MAP	Maximum A Posteriori
MW	Microwave : 2300W
MS	Multi State
NILM	Non-Intrusive Load Monitoring
OW	Observation Window

PC	Desktop Computer
PV	Photovoltaic
PES	Pre Elimination Step
PMF	Probability Mass Function
RAM	Random Access Memory
REDD	Reference Energy Disaggregation Dataset
RF	Refrigerator
SES	Second Elimination Step
SS	Single State
SW	Sliding Window
SC	Subspace Component
TP	True Positives
TV	CRT Television
USA	United States of America
WM	Washing Machine

Symbols:

A	Affinity matrix
σ	Affinity scaling factor
A_{ET}	Average execution time
A_{pd}	Average accuracy of power assigning
λ_i	Average amplitude of i^{th} SC
A_{F_m}	Average F-Measure
$f_{c(i,n)}$	Center frequency of i^{th} SC at n^{th} time instant
$\mathbf{X}$	Data window (1×10 vector)
D	Distance matrix
q_i	i^{th} eigenvector of ACM of $\mathbf{X}$
$F_{m\_c_j}$	F-Measure value of c_j
$Z_{1,.,i}$	Set of SCs up to i^{th} SC of OW
i	Iteration number; SC number
$\gamma_{c_{j,i}}$	Percentage LHV of c_j after i^{th} iteration
N	Length of a SW
L	Normalized laplacian matrix
$\tilde{N}$	Number of SCs
K	Number of clusters
X_K	K^{th} eigenvalue of L in ascending
c_j	j^{th} Possible turned ON *appliance/mode* combination
θ_i	Phase angle of i^{th} SC
$A_{pa\_c_j}$	Power assigning accuracy for c_j
$p_k(t)$	Power consumption of k^{th} appliance at time t
$s(t)$	Solar power output at time t
z_i	i^{th} SC of OW
n	Time instant
$P(t)$	Total power consumption at time t
k_T	Number of turned ON appliances at time t

1. Introduction

Increasing penetration of unpredictable renewable energy sources such as solar photovoltaic (PV) and wind energy have paved the way for many applications of Demand Side Management (DSM) [1]. Due to the intermittent and variable nature of the generation, maintaining the second-by-second balance between the generation and the demand have become a challenging task, unless expensive reserve services are maintained [2, 3]. As an economical solution, a DSM application called Demand Response (DR) through Direct Load Control (DLC) has been introduced [4–7]. DLC tries to adjust the demand either by shifting or reducing the consumption in a way that the available generation can be employed efficiently while maintaining a minimum reserve [8]. Furthermore, during a period where network asserts are over-loaded, DLC could be used to minimize distribution losses.

In DLC, utility is directed to shape the customer energy consumption profile by remotely controlling each customer's pre-agreed set of controllable appliances such as heat, ventilation, air-conditioning and smart systems. In this paper, these controllable loads are called as non-critical loads. Even though a smart meter connected at the consumer premises could make the non-critical loads flexible, unless utilities have an idea about the amount of DR available at a given time, the utilities will have to operate expensive reserve services to maintain the second-by-second balance between the generation and the demand [9, 10].

In order to estimate the amount of DR available at a consumer premises, individual load activities should be monitored[11–14]. For this purpose, both non-intrusive load monitoring methods (NILM) as well as intrusive load monitoring (ILM) methods can be suggested. In general, NILM methods have a number of advantages over ILM methods. If ILM is used, the different appliances connected to the Home Area Network (HAN) should send power measurements from each and every appliances to the smart meter continuously. Therefore to implement DR activity such as direct load control with ILM, a bi-directional communication link with high bandwidth is required. Whereas, using a NILM method, only a uni-directional link with a low bandwidth is adequate. Furthermore, the NILM method could be built in to a smart meter. It would be able to detect devices as well as faults and improve safety; increasing safety.

Non-Intrusive Load Monitoring (NILM) methods [15] are widely studied and utilized in which, only the total power at the entry point to the consumer premises is monitored to find the load activities[16]. Due to its both low cost and complexity, numerous NILM methods have been proposed in the literature [11, 17–24]. These methods enable the identification of turned ON appliances inside a customer premises with their respective power levels non-intrusively.

However, to the best of authors' knowledge, most of the aforementioned NILM methods are unable to identify the individual appliance power levels accurately under the presence of multi-mode appliances such as Washing Machines (WM) and Dish Washers (DW). Further, none of the existing NILM methods have considered the possibility of having a residentially installed solar panels. Furthermore, none of the existing NILM methods have been tested for their

applicability under a large number of houses to estimate the total non-critical load that can be shed (i.e. DR) at a given time instant as well as one day ahead.

As a remedy to these common drawbacks of existing NILM methods, this paper introduces a novel NILM method which extends the previously proposed NILM method in [18] by the authors. The proposed NILM method relies on a Karhunen Loéve expansion (KLE) based subspace separation method [18, 23] which successfully operates even with only active power measurements collected at a low sampling rate (slower than 1 Hz).

In the proposed NILM method, first, individual appliance operating mode identification technique have been formulated based on spectral clustering and KLE. Through this proposed technique, not only the turned ON appliances, but also the operating mode and power consumption level of each turned ON appliance could be detected at a given time. This stage is essential in determining the total residential critical load and non-critical load power demand values. Also, it plays a vital role in determining appropriate load scheduling schemes under DLC [25].

Further, due to increasing trend of using residentially installed solar PV units, the proposed NILM technique is extended to identify the solar power influx while simultaneously identifying the turned ON appliance and their operating modes as well as their power levels [26–28]. This is achieved by simply measuring the total active power profile at the entry point. This will allow utilities to monitor and predict latent demand [29, 30]. The latent demand has introduced one more variable into reserve calculations thus required to maintain more reserve. Therefore, accurately knowing the latent demand enables the utility to further reduce expensive reserve services.

Moreover, the proposed NILM method have been tested and validated for its scalability under a large number of houses to estimate the total non-critical load (i.e. DR), critical load and solar generation at a given time instant as well as one day ahead [27, 31]. Knowledge of the current DR value will enable the system operator to calculate the economic dispatch [32] solution while maintaining minimum energy reserve services. Further, through the predicted DR profile (one day ahead), unit commitment can be planned appropriately [28, 33–36].

2. The Overview of the Proposed Method

There are a number of steps in the proposed NILM method utilized to identify turned on appliances and to predict the total critical and non-critical power demands under residential solar power influx. These steps are shown in Table 1.

Table 1: The main steps in the proposed NILM method

Training Process	1.	Creation of an appliance specific active power profile database.
	2.	Construction of the appliance signatures.
	3.	Construction of the solar power influx signature.
Matching Process	1.	Feature extraction from the aggregated power profile.
	2.	Identification of turned ON appliances, their operating modes and power consumption levels and solar power influx for each residence.
	3.	Identification and prediction of total critical and non-critical load power demands for a cluster of Houses.

3. Training Process

3.1. Creating Appliance Active Power Profile Database

In order to initiate the learning phase of the proposed NILM method, it is required to have a set of pre-observed power profiles per each individual appliance. These set of appliance specific power profiles form the appliance active power profile database.

As mentioned in the Section 5.1, case studies presented in this paper have utilized the data taken from two online databases collected from German and US households. In these databases, individual appliance power profiles are given for a duration of few months. Out of these power profiles, few weeks of data was selected for the training process. Thereafter, by comparing each individual profile with a threshold value, power profile segments corresponding to the turned ON state of each appliance were extracted to form the appliance active power profile database. In other words, this emulates the creation of the global database for this case study. So, in that context, creating the appliance active power profile database was quite straightforward.

When this method is deployed in practice, the process behind creating the appliance active power profile database can be carried out using the hardware setup proposed in Figure2. Here, in each household, a smart meter with a processor unit that performs the NILM algorithm and a Home Area Network (HAN) is required. Once this residential NILM unit is installed, creating appliance active power profile database is initiated.

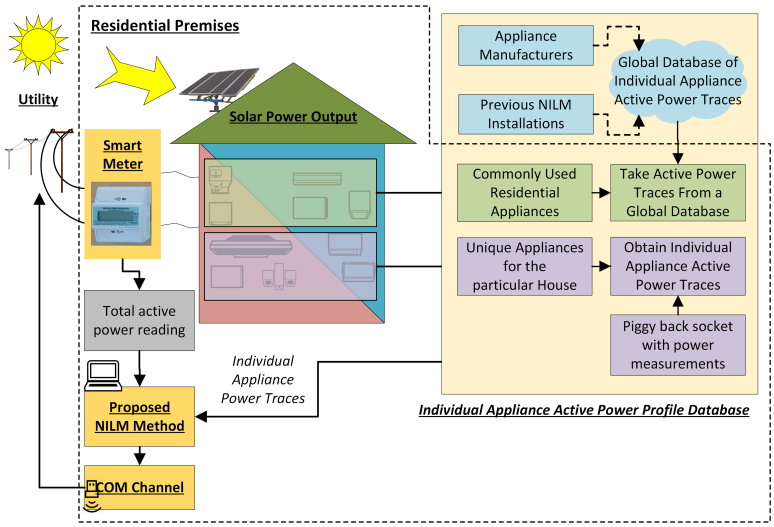

Figure 2: Proposed Hardware Architecture and the Process of Appliance Active Power Profile Database Creation

Since most of the appliances are commonly used across many households, for a large scale implementation, training phase power profiles for such common appliances can be taken from a global database. This global database could be developed using the data collected from previously NILM implemented households as well as using the data taken directly from the appliance manufacturers. It is anticipated that many appliance manufactures will provide factory test power profiles for their product appliances. This database can be continuously updated from a central server according to customer trends and new information received from the customer side and be conveniently downloaded to the NILM equipped smart meter. Therefore, the installation, deployment and operation by the full purview of the utility. In addition the mass deployment and scalability is very convenient.

Apart from that, training power profiles of unique appliances for the considered household that are not captured in the database should be measured individually by turning each of them ON and observing their power profiles for few cycles. In order to capture these sample power traces for the training phase, piggy back sockets with power measurements could be utilized. When this stage is completed, the created appliance active power profile database will contain the training power traces for each and every appliance in the considered household. Further, any unique appliance identified and trained on site can be added to the global database which will continue to grow. As time progresses there would be less likelihood of encountering devices not in the global database as it continues to be updated in this manner.

Here, it should be noted that, piggy back sockets with power measurements will be utilized only in the training phase, for few appliances, for a small time

duration. From there onwards, since the proposed NILM method can monitor the appliances non-intrusively, there will be no use of any intrusive - appliance specific sensors or high bandwidth communication links.

3.2. Construction of Appliance Signatures

For the appliance identification under NILM and for an appliance operating mode identification, two different types of signatures based on spectral features and operating modes were constructed per each appliance.

3.2.1. Spectral Features of Individual Appliances

The low-frequency active power signals of individual appliances were obtained using the method outlined in Section 3.1. First, each active power signal was split into sliding windows (SWs) of 10 samples. Then from each SW, 5 uncorrelated spectral components which are referred as subspace components (SCs) were extracted using the Karhunen Loeve Expansion (KLE) based method [18, 22, 37] described in Appendix A. Here, the KLE based spectral feature extraction method was used as unique signature information of active power signals might not be apparent in the time domain profiles due to their low sampling rate. KLE allows the extraction of hidden features of time domain active power signals by utilizing their uncorrelated spectral components [18, 23, 38]. This process is shown in Figure3.

A given SC is then further decomposed to generate more SCs to improve the resolution. Therefore the KLE was reapplied to each of the original five SCs to create three SCs from each of the original five SCs. Finally, KLE breaks down a given SW into 15 (3×5 SCs at two levels) uncorrelated SCs. Now, each new SC has a very narrow bandwidth which in-turn increases the resolution of the subspace separation procedure.

3.2.2. Operating Modes of Individual Appliances

Appliances can be categorized as 'single state' (SS), 'continuous varying' (CV) and 'multi state' (MS) appliances [18]. The active power consumption of an appliance falling into each of these categories are shown in Figure4.

Multi state appliances have different operating modes/states and each mode consumes different power profiles. For example the active power profile in Figure4 (c) has four different modes/states (denoted by WM_1, WM_2, WM_3, WM_4). Similarity of SWs of same operating mode is much higher than the similarity of SWs of different modes.

In order to infer the current operating modes in a given appliance, signatures associated with its each mode were identified. This was done by exploiting the fact that signatures of the same mode are likely to have high connectivity in terms of spectral content. Due to its inherent ability to identify nonlinear connected structures, spectral clustering [39] was used in this work to cluster signatures based on the mode of operation for a given appliance. Then SWs corresponding to a given operating modes were clustered into one group. In order to appropriately group them into its operating modes using spectral clustering, the algorithm given in Appendix B was used.

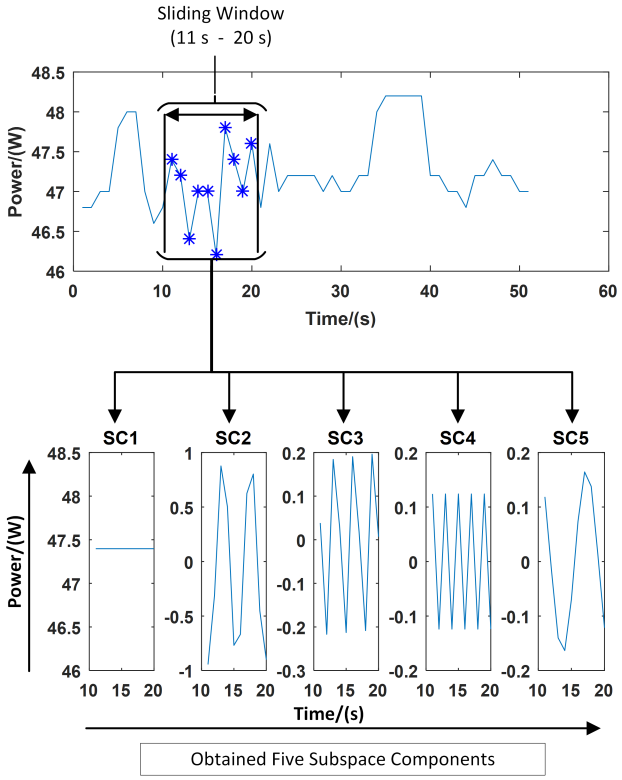

Figure 3: Subspace components decomposition process for the CRT Monitor

For each appliance, the KLE coefficient of all SCs of all SWs were labeled according to the frequency and the identified operating mode. Theses KLE coefficients were used to form a set of probability mass functions (PMFs). Finally, appliance signature database was completed with the constructing relevant PMFs for all appliances.

3.3. Construction of the solar power influx signature

In order to identify the amount of solar power influx coming from the residentially installed solar panels, it was considered as a separate appliance with a negative active power consumption. The Signature for the solar panel was created through following the same procedure which was followed in creating any other appliance signatures. In there, assuming solar power influx does not change during a given SW [40], the spectral power content of frequencies (f) other than 0 Hz were neglected in the constructed Signature. Figure5(b) shows the solar power signature constructed using ten days of solar power profiles.

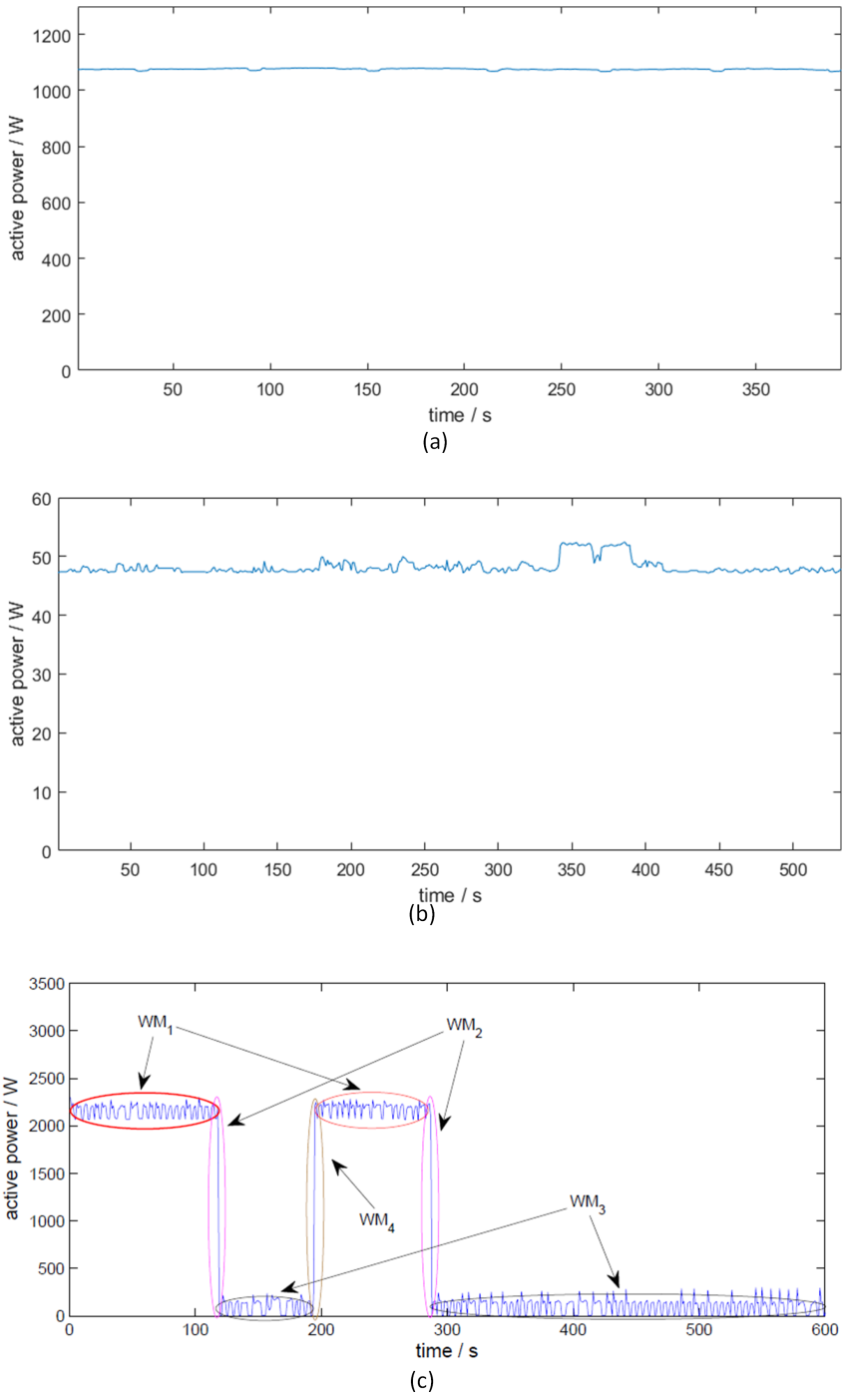

Figure 4: (a) SS appliance Water Kettle, (b) CV appliance LCD TV and (c) MS appliance Washing Machine

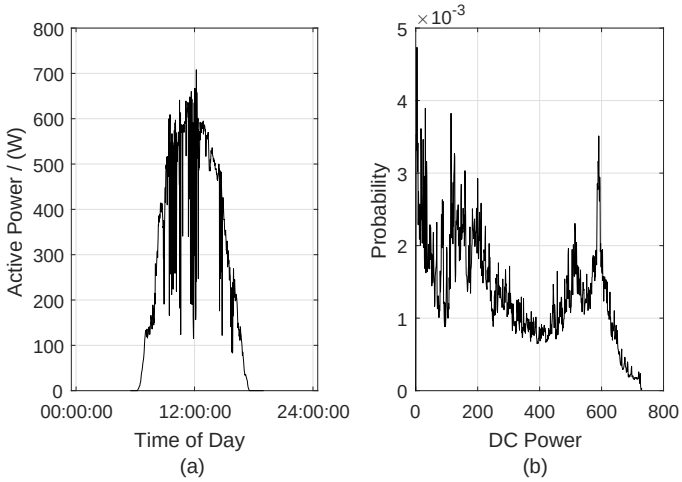

Figure 5: (a) Solar Power Influx in One Day and (b) Solar Power Signature

4. Matching Process

During this phase, the aggregated active power signal measured by the smart meter was considered. First it was partitioned into non-overlapping windows of 10 samples. In this phase, such a window is referred to as an observation window (OW). Then for each OW, 15 number of uncorrelated SCs were extracted using the KLE. SCs of a given OW were sorted in the descending order of dominance in terms of absolute amplitude. It should be noted that the first SC of any OW is the 0 Hz frequency.

For all time periods, the aggregated active power drawn is equal to the total active power consumption of all the turned on appliances at the time slot considered minus the solar power influx to the given house. That is, the aggregated power is simply a linear addition of the individual power contributions of each turned-on appliance and solar power input (considered as an appliance with negative power consumption) at any given time.

Considering the fact that an SC with frequency f in a given OW can only be generated from a linear addition of the individual SCs with the same frequency f out of the turned on appliances in that OW, the identification of actual turned on appliance combination in a given OW was obtained by matching of each SC of a given OW with the linear addition of individual appliance SCs that are already stored in the signature database. As there are a large number of appliance combination candidates to be considered to find the best matching appliance combination in the given OW, an iterative process was developed. The main work flow of this matching process is presented in the Algorithm 1. As shown in Algorithm 1, the proposed matching process is an iterative approach whose maximum iteration number equals to the number of SCs of a given OW, i.e. 15. For any given OW, the i^{th} dominant SC was taken for calculations for the i^{th} iteration of the algorithm. It consists of four main steps namely: the pre

elimination step (PES), the first elimination step (FES), the second elimination step (SES) and the Maximum a Posteriori (MAP) estimation.

Algorithm 1 Main Work Flow of the Proposed Matching Algorithm for Turned on *appliance/mode* Identification

1: Set $i = 1$
2: Set $execution = 1$
3: Apply the PES to the given OW and obtain S_0;
4: **while** $execution$ **do**
5: Take i^{th} dominant SC;
6: Apply the FES to S_0 or S_2 and obtain S_1;
7: Apply the SES to S_1 and obtain S_2;
8: Apply the MAP criteria to S_2;
9: **if** $\gamma > 99\%$ **then**
10: Output: Turned on *appliance/mode* combination and mean solar power influx of the given OW;
11: Set $execution = 0$;
12: **else**
13: $i = i + 1$
14: **end if**
15: **end while**

4.1. Pre Elimination Step

A pre-elimination was conducted to reduce the number of possible *appliance/mode* combinations which needs to be considered in the iterative matching process in Algorithm 1 (while do loop). If the mean power level of a given OW is less than the summation of the minimum mean power level of all appliances in a given *appliance/mode* combination (except solar influx) and the maximum possible power influx of the solar panel (as solar is considered as a negative load), that *appliance/mode* combination was eliminated from the matching process. This is given by the line 3 of the Algorithm 1; where S_0 refers to the set of possible combinations that satisfy the above criteria within a given OW.

4.2. First Elimination Step

The first elimination step exploits the triangular law of complex numbers to eliminate the combinations. At the first iteration, the FES was carried out for the reduced set of possible combinations obtained from the PES (denoted as set S_0). In all other iterations, the FES was applied to the reduced set of possible combinations obtained from the second elimination step (denoted as set S_2).

For a given SC of frequency f of a given OW, for a selected combination, if the maximum power contribution of the same frequency f of each appliance that make up the combinations (without solar panel), once linearly added cannot match (or is less than) the power at that SC of the given OW, clearly that combination cannot generate the power required to the given OW. This is given by the line 6 of the Algorithm 1.

4.3. Second Elimination Step (SES)

In the second elimination step, a likelihood estimation was carried out to determine the likelihood of getting the real and imaginary value of the observed SC of frequency f from a given combination. Therefore, a joint likelihood function of the real and imaginary values of SCs for a given *appliance/mode* combination was generated. In order to generate such a combinational joint likelihood function, joint likelihood functions for individual appliances of the given combination were first generated based on SCs of frequency f of their SWs.

The new combinational joint likelihood function for the given combination was thereafter calculated using the 2D convolution operation of the joint likelihood functions of individual appliances of the given combination. If the likelihood value for real and imaginary value of given SC of the OW was close to zero, such combinations were eliminated. This is given by the line 7 of the Algorithm 1.

4.4. MAP Estimation

At the i^{th} iteration, there may be multiple combinations that would produce the first i dominant SCs of a given OW. It is required to find the most likely combination c_j for the given Z_i (Z_i represents first i dominant SCs of the given OW). By Bayes's rule we have,

$$P(c_j|Z_i) = \frac{P(Z_i|c_j)P(c_j)}{P(Z_i)}, \tag{1}$$

where $P(Z_i|c_j)$ denotes the likelihood value (LHV) of producing first i dominant SCs of a given OW using SCs of the given combination c_j. Further, term $P(c_j|Z_i)$ represents the LHV of c_j as being the turned-on *appliance/mode* combination of the given OW, when its first i dominant SCs are considered. The LHV of combination c_j occurring in the given OW, is denoted by $P(c_j)$. This depends on the usage behavior pattern of the combination c_j with respect to time of a day. In this paper, such usage behavior patterns were not taken into account and assumed that the LHV of all $P(c_j)$ were equally likely. Since $P(Z_i)$ is common to all combinations and all $P(c_j)$ are equally likely, they do not make any difference to the rank when ordering 'likely combinations' in terms of likelihood. Hence, the LHV of $P(c_j|Z_i)$ is linearly proportional to the LHV of $P(Z_i|c_j)$. Since the LHV of producing any SC of the OW from SCs of SWs of a given combination c_j are independent, we have,

$$P(Z_i|c_j) \quad = \quad \prod_{m=1}^{i} P(z_{f_m}|c_j), \tag{2}$$

where $P(z_{f_m}|c_j)$ denotes LHV of producing m^{th} dominant SC, i.e., z_{f_m} of a given OW using SCs of the given combination c_j. The LHV of $P(z_{f_m}|c_j)$ was determined from the generated joint likelihood functions at the SES.

At the i^{th}, if the percentage LHV of the most likely combination c_j, which

has the highest LHV out of the remaining combinations, was greater than a pre-defined threshold or confident level, then the combination c_j was selected as the identified or estimated turned-on *appliance/mode* combination. Once this condition was satisfied, the execution of the algorithm was terminated. The percentage LHV for most likely combination (denoted as $\gamma_{c_{j,i}}$) at iteration i is given as,

$$\gamma_{c_{j,i}} = \frac{\max(P(Z_i|c_j)}{\sum_{j=1}^{l} P(Z_i|c_j)} \times 100\%, \tag{3}$$

where l is the number of combinations of the set S_2 at iteration i.

If the termination condition was not satisfied by any combination after all 15 iterations (i.e. $i = 15$), then the combination c_j with the maximum LHV (i.e. $\arg\max_{c_j} P(Z_{15}|c_j)$), was selected as the identified or estimated turned-on *appliance/mode* combination. In this paper, 99% confidence level was selected as the pre-defined threshold.

4.5. Power Level Disaggregation

Corresponding mean power levels of the identified operating mode combination were considered as disaggregated mean power levels of the identified turned on appliances in a given OW. Moreover, if the solar panel is operating in a given OW, its mean power equals to the difference of the mean power of the given OW and the summation of the disaggregated mean power of the identified turned on appliances in the given OW.

4.6. Identification of Total Critical and Non-Critical Load Power Demand and Prediction

The NILM algorithm described in Section 3 & 4 estimates the turned ON *appliance/mode* combination, and the residential solar plant output in a given house at each time instant. Furthermore, it also gives the power disaggregation among the identified turned ON appliances in that house.

However, for DSM programs like DLC, such detailed appliance level power consumption data is not important. For such applications, knowing only the non-critical loads that can be shed and critical loads that needs to be maintained of a house is sufficient [41]. So, in such occasions, user signs an agreement with the utility defining a set of appliances as non-critical appliances (E.g. Refrigerator, Cookers, Air Conditioners, Heaters, etc.). Therefore, using the proposed NILM method and a predefined categorization of each residential appliance as either a critical or non-critical appliance, the total residential power demand profile was disaggregated into three groups as critical, non-critical and solar power profiles [42].

Once the proposed NILM algorithm is evaluated on the houses of a region, the total estimated critical, non-critical and solar power profiles of that region are found by aggregating respective power profiles estimated for each house. The knowledge of the total non-critical power demand of all the houses connected to the power system give the total power which can be turned OFF by the system operator remotely in case of a system emergency [12]. So, it leads to

maintaining less energy reserve services and more optimum economic dispatch solutions [32].

Further, in the unit commitment problem [12, 33], the sequence of the power generating units which should be brought into match the varying demand is determined one day ahead using the predicted total power demand profile. This is usually done using a prediction algorithm based on few recent past total power demand profiles [43]. However, with the proposed NILM method, in addition to the total power demand, the power profiles of estimated total critical, non-critical and solar influx are also available. So, with this additional information, more optimum unit commitment solution could be obtained. Here a test case was conducted to demonstrate the applicability of prediction algorithms to predict the total critical, non-critical and the solar profiles of aggregated set of houses after observing these profiles (estimated by the proposed NILM method) for few consecutive days in each house.

Here, First, the total residential non-critical demand profile was identified through evaluating the proposed NILM method. Next, this profile was observed for four consecutive days in all the houses. Then a variance minimization based method influenced by the sensor fusion technique [44] was utilized to predict the most probable total non-critical power profile for the fifth day. The same strategy was utilized for the prediction of the total critical power profile and the total solar power influx (see Section 5.5). In the literature, this solar prediction problem is a well studied problem incorporating only the weather reports [45, 46] but, without estimated solar power profiles of few previous days. So it is clear that this proposed NILM algorithm can supply important information for such solar prediction mechanisms as well.

5. Case Study

Three case studies were conducted. In the first case study, the ability of disaggregating solar and individual appliance power profiles of a real household was considered. Then, case study 2 was carried out to evaluate the ability to estimate critical, non-critical and solar power influx profiles for a aggregated set of 400 houses by evaluating the proposed NILM algorithm in each house. The ability to predict the total critical and non-critical load profiles were studied in case study 3 after obtaining estimates for critical and non-critical power profiles for few consecutive days of all 400 houses.

5.1. Appliance and Solar Influx Measurement Datasets Used

Two publicly available datasets containing individual appliance power profiles collected from German and US households were considered for this study. They are *Reference Energy Disaggregation Dataset (REDD)*[47] and *Tracebase* [48] respectively. Further, solar power data obtained at a Solar Power Station in California, USA were used for performance validation of the proposed NILM method. For subsequent studies, twenty appliances from the *Tracebase* dataset were chosen and were categorized into critical and non-critical appliances.

Using individual appliance power profiles taken from the *Tracebase* dataset and solar power influx data, 400 different virtual houses were constructed for this study. These houses were generated by selecting daily appliance and solar data windows randomly and by shifting daily appliance power profiles randomly to ensure uniqueness among each household. Then, for each house, six appliances were chosen from each appliance category randomly so that there are twelve appliances per house. Therefore, each virtual house is modeled as having residential solar influx as well as two or more appliances from each appliance category [18]: Single State (SS), Multi-Sate (MS), and Continuously Varying (CV). Some of the appliances selected from each category are given in Table 2.

Table 2: Appliance Categories and Some Selected Exemplary Appliances

Appliance Category	Selected Appliances	
	Critical Appliances	Non-Critical Appliances
Single State (SS)	60 W & 100 W Lamps (LM1 & LM2)	Microwave Oven (MW), Water Kettle1 (WK1)
Continuously Varying (CV)	CRT Television (TV), Desktop Computer (PC)	Cooking Stove (CS)
Multi State (MS)	Dish Washer (DW)	Refrigerator (RF), Washing Machine (WM)

5.2. Performance Metrics Used

Following performance metrics were used in case studies:

5.2.1. Average F-Measure (A_{F_m})

The F-measure ($F_{m\_c_j}$) [49] was used to evaluate the performance of identification of turned ON *appliance/mode* combination c_j. It is given by,

$$F_{m\_c_j} = 2TP/(2TP + FN + FP), \tag{4}$$

where for each identified turned ON c_j, the TP, FN and FP are the true positives, false negatives and false positives. The average F-measure (denoted as A_{F_m}) was obtained by averaging $F_{m\_c_j}$ (over all c_j) for a given aggregated active power signal.

5.2.2. Total Power Correctly Assigned (A_{pd} and A_{pf})

To evaluate the performance of the power disaggregation, the "Total Power Correctly Assigned ($A_{pa\_c_j}$)" metric described in [15, 47] was used. Metric $A_{pa\_c_j}$ is formally defined for *appliance_mode* combination c_j as follows [47]:

$$A_{pa\_c_j} = \left[1 - \frac{\sum_{t=1}^{T}\sum_{i=1}^{n}\left|\hat{y_t}^{(i)} - y_t^i\right|}{\left(2\sum_{t=1}^{T}\sum_{i=1}^{n} y_t^i\right)}\right], \tag{5}$$

where $\hat{y_t}^{(i)}$ denotes the calculated mean power level of the proposed method for i^{th} appliance at the t^{th} OW while y_t^i denotes the measured mean power level for i^{th} appliance at the t^{th} OW in a given aggregated signal. The average $A_{pa\_c_j}$ over for all c_j in a given aggregated active power signal is denoted as A_{pd}.

5.2.3. Average Execution Time (A_{ET})

All algorithms in this paper were executed on a workstation with Intel Core i7 processor with 16.00 GB RAM running at 2.2 GHz, with MAC (EI Capitan) operating system. The average execution time A_{ET}, taken to process an OW to generate the NILM result was used to demonstrate the speed of the solution.

5.2.4. Mean Absolute Error (MAE) and Mean Absolute Percentage Error (MAPE)

In order to evaluate the performance of estimation/prediction algorithms (in Case Study 2 & 3), MAE and MAPE metrics proposed in [50] were used.

5.3. Case Study 1

This case study was performed to demonstrate the viability of the proposed NILM algorithm to accurately identify the turned ON *appliance/mode* combination and to estimate residential individual appliance and solar power contribution to the residential total power consumption profile. All six houses in the REDD database were used in this case study after adding a selected solar power profile for each house for each day. However, most of these cases, the amount of generated solar power is less than the power consumed by appliances. In many practical situations, solar generation exceeds the consumption, even when household appliance is used. Therefore, we selected solar power profiles, in order to viable with this practical condition.

Four weeks of active power data for each house in the REDD database was used in this case study. Figure6 shows the net power flow of House 6 analyzed for a selected day to highlight the total power fluctuation that ranges from positive to negative values throughout the day. Robustness of an NILM algorithm to correctly estimate active loads under both positive and negative net power flow is paramount due to the high penetration of solar power/renewables in modern households. The circuit/device specific data of first 10 days was used for the training phase (for generation of appliance signatures). For next 18 days, the proposed NILM method was applied to the active power signals measured from these households.

5.3.1. Results and Discussion

The turned ON *appliance/mode* identification accuracy and their mean power disaggregation accuracy (including the accuracy of solar power extraction) of the proposed method for test signals of each selected houses are presented in Table 3. This shows that, when actual active power signals measured from most of the test households were used, turned on *appliance/mode* combinations were identified with more than 83% accuracy in terms of A_{f_m} and their power disaggregation was conducted with more than 82% accuracy in-terms of A_{pd} by the proposed NILM method. Further, as obtained average execution time values are less than the sampling time of the power measuring device (3 s), it confirms the viability of deploying this algorithm in real-time.

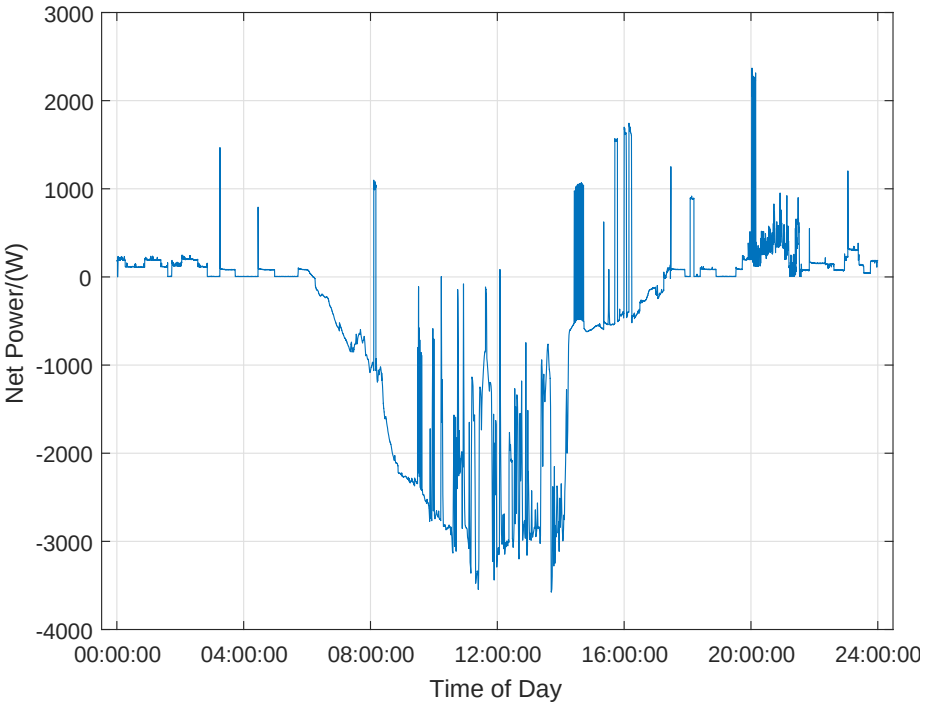

Figure 6: Net power flow of House No. 6 Day No. 21

From the obtained accuracy levels shown in Table 3, it is clear that in a given house, for a certain duration, if the appliances are known and solar influx exists, still utilizing the proposed NILM algorithm one can extract each appliance power profile, and solar power output separately from the total power consumption profile of that house. By categorizing all the appliances in a house into critical and non-critical loads, using the NILM result obtained, estimated critical, non-critical and solar power profiles of that house were obtained. Figure7 presents the actual and estimated critical, non-critical and solar power profiles of the House 6 during a selected day.

5.3.2. Comparison with State of the Art

In this case study, as a benefit of using the publicly available *REDD* dataset, and the use of common accuracy metrics such as the F-Measure value (A_{f_m}) and the Total Power Correctly Assigned metric (A_{pd}), enabled a direct comparison with some of the state of the art NILM algorithms.

First, authors have used the NILM Tool-Kit (NILMTK) made available in [51] for the dataset conversion and in data pre-filtering stages. But, due to the limitations in the NILMTK software architecture, reusing the existing NILM algorithms available in NILMTK, under the presence of externally inserted solar power influx was not possible. As a result, for this comparison, authors have

Table 3: Appliance identification accuracy, appliance/solar power disaggregation accuracy, and average execution time for an OW, of aggregated test signals used in Case Study 1

House	A_{F_m} (%)	A_{pd}(%)	A_{ET} (s)
House 1	88.7	87.1	2.22
House 2	89.1	88.5	2.21
House 3	83.8	82.9	1.29
House 4	86.1	85.9	1.62
House 5	78.4	77.3	1.88
House 6	84.1	82.4	1.87

directly used the accuracy levels of selected set of state of the art NILM methods, as reported in the literature.

Here, it should be noted that, all of these NILM methods which were used in this comparison have utilized the same REDD dataset without considering a solar influx. Further, it was observed that, some NILM methods found in the literature are more focused on appliance combination identification while the others are more focused on power level disaggregation. Therefore, most of the NILM methods in the literature have either used the F-Measure value (A_{f_m}) or the Total Power Correctly Assigned metric (A_{pd}) separately. In contrast, the NILM method proposed in this paper have used both these metrics. So, in the first stage of the comparison, achieved F-measure values were compared.

NILM approach previously proposed by the authors using a KLE based low-resolution spectral decomposition technique has been discussed in [18]. In [52], supervised Graph Signal Processing (GSP) based NILM method has been introduced. Additive Factorial Hidden Markov Model (FHMM) based benchmark NILM algorithm has been introduced in [53]. Further, event classification technique based on a Decision Tree (DT) classifier has been proposed in [54]. Furthermore, [55] explores multi-label classification (ML-KNN) based NILM method using both time domain and wavelet domain feature sets. It should be noted that none of these NILM algorithms have considered the solar influx. Further, they have only considered a certain set of appliances when evaluating the F-Measure value. In contrast, the proposed NILM method have been evaluated for all houses of the *REDD* dataset, considering all appliances in each household even including a solar power influx.

Overall average F-measure values obtained by these diverse set of state of the art NILM methods including the NILM method proposed in this paper are summarized in the Table 4. As can be seen from the table the A_{f_m} percentage value is highest when using the proposed NILM method.

In the next comparison, achieved individual appliance power level disaggregation accuracies given by the metric Total Power Correctly Assigned (A_{pd}) were compared. For this comparison, different state of the art NILM methods including the proposed NILM method in this paper was utilized. Table 5 summarizes the obtained results from this comparison. The different NILM approaches used for this comparison are summarized in the following paragraph.

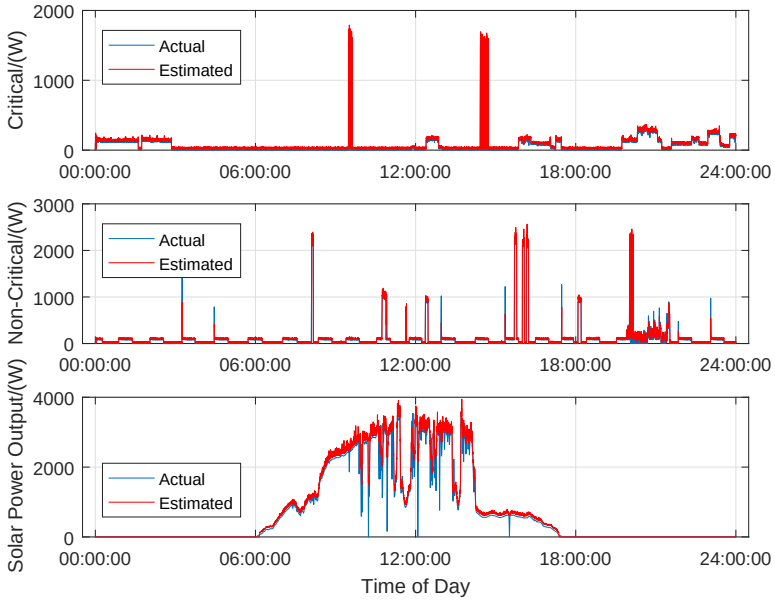

Figure 7: Actual vs Estimated Critical, Non-Critical and Solar Power Profiles of House No. 6 Day No. 21

In [56], for the load disaggregation task, Deep Sparse Coding (SC) approach has been introduced based on Exact Solution technique. For the same task, another three avenues have been explored in [57], [58] and [47] which uses 'Powerlets' Learning (PED), Temporal Multi-Label Classification (ML) and Factorial HMM (FHMM) respectively. Moreover, Hidden Semi-Markov Model based technique, named Factorial-Hierarchical Dirichlet Process (F-HDP-HSMM), has been used in [59] for this power level disaggregation task.

From this comparison, it was observed that F-HDP-HSMM method proposed in [59] has slightly outperformed the proposed NILM method. However, as reported in [47, 56–59], even when evaluating the A_{pd} value also, these other NILM methods have only utilized a limited number of appliances in few households. In contrast, the proposed NILM method was evaluated on all six REDD houses, disaggregating seven highest power consuming appliances and the solar power influx.

In conclusion, both appliance identification accuracy and the power level disaggregation accuracy of the proposed NILM method were either comparable or superior to the existing state of the art NILM methods.

5.4. Case Study 2

This case study is presented to evaluate the ability of the proposed NILM method in identifying the total critical, non-critical and solar power profiles for a aggregated set of 400 houses. As discussed in Section 5.1 a database containing appliance level power consumption profiles of 400 houses were constructed.

Table 4: Comparison of Obtained F-Measure Values

NILM Method	A_{f_m} /(%)	Remarks
Proposed method	**85.0**	**Using all appliances in all six houses with solar influx.**
Spectral Decomposition [18]	79.7	Using all appliances in all six houses.
Supervised GSP [52]	64.0	Using only 5 most performing appliances in Houses 2 & 6.
Additive FHMM [53]	71.3	Using only 7 most performing appliances
Supervised DT [54]	76.4	Using only 9 most performing appliances.
Multi-Label KNN [55]	59.1	Using only 9 arbitrary selected appliances.

5.4.1. Results and Discussion

After evaluating the proposed NILM algorithm on all 400 houses, each estimated critical, non-critical and solar power profiles for each house were aggregated to find the total estimated critical, non-critical and solar power profiles of the whole set of 400 households. Then those three estimated profiles were compared with the corresponding actual power profiles. These estimated and actual power profiles for Day 3 are shown in Fig. 8. Obtained MAPE values for estimation are shown in Table 6.

From Fig. 8 it is clear that obtained estimations of critical, non-critical and solar power profiles of aggregated set of 400 houses are accurate enough when compared to actual values. Moreover, instead of only utilizing daily total load profile, these three estimated profiles can give the amount of DSM available to support the grid in case of a system emergency.

Table 5: Comparison of Obtained Power Disaggregation Accuracy Values

NILM Method	A_{pd} /(%)	Remarks
Proposed Method	**84.0**	**For all six houses with solar influx**
Spectral Decomposition [18]	81.0	For all six houses
Exact Deep SC [56]	66.1	Using only Houses 1, 2, 3, 4 & 6 [56].
Powerlets-PED [57]	46.5	
Temporal ML [58]	53.3	
Factorial HMM [47]	47.7	
F-HDP-HSMM [59]	84.8	Using only 5 appliances in the Houses 2 [60].

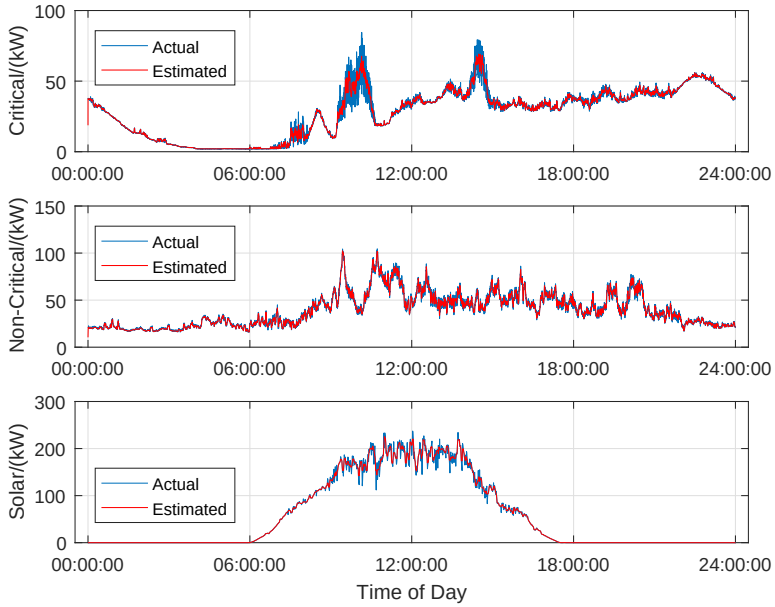

Figure 8: Actual vs Estimated Critical, Non-Critical and Solar Power Profiles of Aggregated 400 Houses in Day No. 3.

Table 6: Obtained Daily MAPE Values for Estimated Total Critical, Non-Critical and Solar Influx Profiles of 400 Houses

Day No.		01	02	03	04	05
$MAPE/(\%)$	Critical	5.23	6.01	4.02	4.51	4.98
	Non-Critical	4.25	3.98	3.76	4.88	5.02
	Solar	5.22	5.86	4.75	4.98	5.10

5.5. Case Study 3

Here the predictability of critical and non-critical power profiles have been explored when it has been estimated for few consecutive days. The dataset of 400 households constructed as described in Section 5.1 was utilized in this case study as well. Since this dataset has been constructed by selecting appliance power profiles of 10 consecutive days, it was utilized in developing and testing the prediction method proposed in Section 4.5 to find the next day's total critical and non-critical power profiles, once estimates of those are known for four consecutive days.

5.5.1. Results and Discussion

Fig. 9 shows the comparison of the predicted and actual total non-critical power profile of 400 houses on the Day 5 using the estimated household data of Day 1 to Day 4. The same experiment was carried out for predicting total non-critical and critical power profiles of 400 houses during Day 6 to Day 10.

Table 7: Prediction Accuracies in Terms of Error Percentages

House	Non-Critical Power		Critical Power	
Day	MAE (kW)	MAPE(%)	MAE (kW)	MAPE(%)
Day 5	3.13	7.71	3.13	8.12
Day 6	3.51	7.19	2.88	9.25
Day 7	4.01	8.96	4.23	7.99
Day 8	3.56	8.54	3.66	7.50
Day 9	2.97	7.51	2.91	7.05
Day10	3.05	7.89	2.75	9.02

In order to evaluate the performance of the proposed prediction strategy, MAE and MAPE metrics described in Section 5.2.4 were used and the obtained results are summarized in Table 7. From the results, it is clear that developed mechanism for predicting next day's total non-critical or critical power profile have the MAE and MAPE values comparable to those of existing total load profile prediction techniques [61].

6. Conclusion

This paper proposes a novel NILM approach with enhanced capabilities not only to identify the turned-on appliances, their operating modes and power consumption levels but also to estimate the amount of solar power influx in the

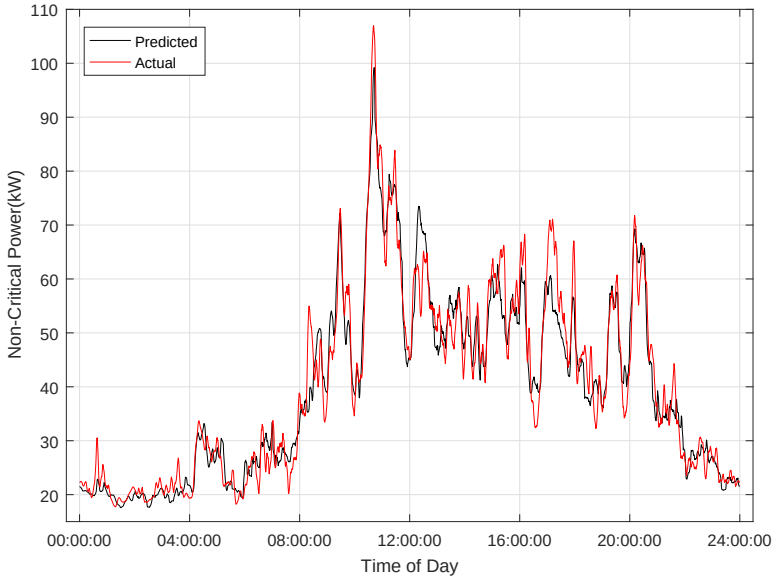

Figure 9: Predicted vs Actual Non-Critical Power Profiles of aggregated 400 Houses

presence of residentially installed solar panel. This ability to identify the individual appliance power as well as solar power contributions in the total active power consumption of a house gives the grid operator the ability to calculate estimated total critical load and total non-critical load profiles together with the total solar power profile for a set of regional households. This has an important practical interest as utilities are reluctant to utilize DLC due to the difficulty of estimating the amount of DR available. Consecutive estimation of non-critical load profile of a set of houses via the proposed NILM strategy enabled employing a confidence based weighting algorithm for prediction of next day's total non-critical load profile. This prediction mechanism as demonstrated in this paper, shows sufficiently high accuracy which allows the utilities to consider DLC when calculating the unit commitment schedule thus eliminating the excessive employment of expensive reserve services.

Appendix A.

If $\mathbf{X} = [X(1)\ X(2)...X(i)...X(N)]^T$ is a sliding window (SW) of an individual appliance or aggregated active power trace, its KLE is given by,

$$\mathbf{X} = Q\bar{x} = \sum_{i=1}^{\bar{N}} q_i^T \mathbf{X} q_i \tag{A.1}$$

where, $q_1, q_2, ..., q_{\bar{N}}$ and Q represents the eigenvectors and the eigenvector matrix of the Autocorrelation Matrix (ACM) of $\mathbf{X}$.

According to (A.1), signal $\mathbf{X}$ was decomposed into $\bar{N}$ number of mutually uncorrelated spectral components which are also known as Subspace Components (SCs) of $\mathbf{X}$. Here, q_i can be thought of as a narrow band eigen-filter whose output is sinusoidal with a center freq of f_{ci} and phase angle of θ_i. Then, the average amplitude of SC which is incidentally the eigenvalue λ_i and the phase θ_i was converted into rectangular form (Re_i, Im_i) to form the complex features for each SC.

Appendix B.

Spectral Clustering is a connectivity based segmenting tool which is capable of segmenting activities into classes based on similarities in dynamics [39]. Even though most clustering methods rely on a pre-training phase to perform segmentation, Spectral Clustering does not require any prior learning. It consists of the three main steps: graph construction, spectral representation, and clustering.

Graph construction: For a given set of n data points to be clustered, a symmetric graph is constructed as a set of nodes with an affinity matrix. Each node corresponds to a data point while the affinity matrix represents the strength of edge links between the nodes. The $n \times n$ affinity matrix is usually defined as

$$A[i,j] = \exp\left\{-\frac{D[i,j]}{2\sigma^2}\right\},$$

where σ is the affinity scaling factor and $D[i,j]$ represents the distance between node i and j. Distance metric is chosen in an application-specific manner. Similarly to [39], in this paper we select σ as the standard deviation of the values in D.

Spectral representation: A new vector representation for each node is defined using the spectrum of the normalized Laplacian matrix L of the constructed graph. First, $L \in R^{n \times n}$ is determined as [39]:

$$L = W^{-1/2}(W - A)W^{-1/2}, \tag{B.1}$$

where W is a diagonal matrix whose diagonal entries are summations of the corresponding columns of A: $W[i,i] = \sum_{j=1}^{n} A[j,i]$. Then, eigenvectors $v_1, v_2, ..., v_m$ corresponding to the m largest eigenvalues of L are used to construct a matrix

$X \in R^{n \times m}$, as $X[:, i] = v_i$. Here $X[:, i]$ represents the i-th column of matrix X. Finally, matrix Y is defined as

$$Y[i, :] = \frac{X[i, :]}{\|X[i, :]\|_2}$$

where $\|\cdot\|_2$ is the Euclidean norm. Further, $Y[i, :]$ and $X[i, :]$ represents i-th row of matrix Y and X respectively. Now, the i-th row of Y, $Y[i, :]$, represents node i in the R^m space.

Clustering: The rows of Y are treated as points in R^m and clustered using the K-means algorithm. Node i is assigned to cluster o if and only if $Y[i, :]$ is assigned to the cluster o. In this paper, the number of clusters (K) is determined based on the eigenvalue difference distribution of the matrix L as follows [39]:

$$K = \arg\max_k(|\lambda_k - \lambda_{k+1}|),$$

where λ_k denotes the k-th largest eigenvalue of L.

In this paper we treat all SWs of a given appliance as nodes of the graph, and the $A[i, j]$ will represent Euclidean distance between SW i and SW j. Then the algorithm returns the SWs of the appliance, appropriately grouping them into the different operating modes.

Acknowledgment

We would like to acknowledge the financial support provided by the National Science Foundation Sri Lanka (Research Grant No: RG/2016/EA & ICT/01).

References

[1] N. Batista, R. Melcio, J. Matias, J. Catalo, Photovoltaic and wind energy systems monitoring and building/home energy management using zigbee devices within a smart grid, Energy 49 (2013) 306 – 315. doi:http://dx.doi.org/10.1016/j.energy.2012.11.002.
URL http://www.sciencedirect.com/science/article/pii/S0360544212008390

[2] E. Reihani, S. Sepasi, R. Ghorbani, Scheduling of price-sensitive residential storage devices and loads with thermal inertia in distribution grid, Applied Energy 183 (2016) 636 – 644. doi:http://dx.doi.org/10.1016/j.apenergy.2016.08.115.
URL http://www.sciencedirect.com/science/article/pii/S0306261916312156

[3] T. Hoogvliet, G. Litjens, W. van Sark, Provision of regulating- and reserve power by electric vehicle owners in the dutch market, Applied Energy 190 (2017) 1008 – 1019. doi:http://dx.doi.org/10.1016/j.apenergy.2017.01.006.
URL http://www.sciencedirect.com/science/article/pii/S0306261917300077

[4] K. Stenner, E. R. Frederiks, E. V. Hobman, S. Cook, Willingness to participate in direct load control: The role of consumer distrust, Applied Energy 189 (2017) 76 – 88. doi:http://dx.doi.org/10.1016/j.apenergy.2016.10.099.
URL http://www.sciencedirect.com/science/article/pii/S0306261916315458

[5] M. Qadrdan, M. Cheng, J. Wu, N. Jenkins, Benefits of demand-side response in combined gas and electricity networks, Applied Energy (2016) –doi:http://dx.doi.org/10.1016/j.apenergy.2016.10.047.
URL http://www.sciencedirect.com/science/article/pii/S0306261916314866

[6] S. Bahrami, V. W. S. Wong, J. Huang, An online learning algorithm for demand response in smart grid, IEEE Transactions on Smart Grid PP (99) (2017) 1–1. doi:10.1109/TSG.2017.2667599.

[7] S. Wang, R. Tang, Supply-based feedback control strategy of air-conditioning systems for direct load control of buildings responding to urgent requests of smart grids, Applied Energy (2016) – doi:http://dx.doi.org/10.1016/j.apenergy.2016.10.067.
URL http://www.sciencedirect.com/science/article/pii/S0306261916315070

[8] J. Thakur, B. Chakraborty, Demand side management in developing nations: A mitigating tool for energy imbalance and peak load management, Energy 114 (2016) 895 – 912. doi:http://dx.doi.org/10.1016/j.energy.2016.08.030.
URL http://www.sciencedirect.com/science/article/pii/S0360544216311331

[9] M. Shad, A. Momeni, R. Errouissi, C. P. Diduch, M. E. Kaye, L. Chang, Identification and estimation for electric water heaters in direct load control programs, IEEE Transactions on Smart Grid 8 (2) (2017) 947–955. doi:10.1109/TSG.2015.2492950.

[10] A. Gholian, H. Mohsenian-Rad, Y. Hua, Optimal industrial load control in smart grid, IEEE Transactions on Smart Grid 7 (5) (2016) 2305–2316. doi:10.1109/TSG.2015.2468577.

[11] A. Cominola, M. Giuliani, D. Piga, A. Castelletti, A. Rizzoli, A hybrid signature-based iterative disaggregation algorithm for non-intrusive load monitoring, Applied Energy 185, Part 1 (2017) 331 – 344. doi:http://dx.doi.org/10.1016/j.apenergy.2016.10.040.
URL http://www.sciencedirect.com/science/article/pii/S030626191631488X

[12] K. Samarakoon, J. Ekanayake, N. Jenkins, Reporting available demand response, IEEE Transactions on Smart Grid 4 (4) (2013) 1842–1851. doi:10.1109/TSG.2013.2258045.

[13] Y. Ji, P. Xu, P. Duan, X. Lu, Estimating hourly cooling load in commercial buildings using a thermal network model and electricity submetering data, Applied Energy 169 (2016) 309 – 323. doi:http://dx.doi.org/10.1016/j.apenergy.2016.02.036.
URL http://www.sciencedirect.com/science/article/pii/S0306261916301593

[14] L. Stankovic, V. Stankovic, J. Liao, C. Wilson, Measuring the energy intensity of domestic activities from smart meter data, Applied Energy 183 (2016) 1565 – 1580. doi:http://dx.doi.org/10.1016/j.apenergy.2016.09.087.
URL http://www.sciencedirect.com/science/article/pii/S0306261916313897

[15] G. W. Hart, Nonintrusive appliance load monitoring, Proc. IEEE 80 (12) (1992) 1870–1891.

[16] S. Biansoongnern, B. Plungklang, Non-intrusive appliances load monitoring (nilm) for energy conservation in household with low sampling rate, Procedia Computer Science 86 (2016) 172 – 175, 2016 International Electrical Engineering Congress, iEECON2016, 2-4 March 2016, Chiang Mai, Thailand. doi:http://dx.doi.org/10.1016/j.procs.2016.05.049.
URL http://www.sciencedirect.com/science/article/pii/S1877050916303854

[17] M.-S. Tsai, Y.-H. Lin, Modern development of an adaptive non-intrusive appliance load monitoring system in electricity energy conservation, Applied Energy 96 (2012) 55 – 73, smart Grids. doi:http://dx.doi.org/10.1016/j.apenergy.2011.11.027.
URL http://www.sciencedirect.com/science/article/pii/S0306261911007240

[18] C. Dinesh, B. W. Nettasinghe, R. I. Godaliyadda, M. P. B. Ekanayake, J. Ekanayake, J. V. Wijayakulasooriya, Residential appliance identification based on spectral information of low frequency smart meter measurements, IEEE Transactions on Smart Grid 7 (6) (2016) 2781–2792. doi:10.1109/TSG.2015.2484258.

[19] S. R. Shaw, S. B. Leeb, L. K. Norford, R. W. Cox, Nonintrusive load monitoring and diagnostics in power systems, IEEE Transactions on Instrumentation and Measurement 57 (7) (2008) 1445–1454. doi:10.1109/TIM.2008.917179.

[20] T. Hassan, F. Javed, N. Arshad, An empirical investigation of v-i trajectory based load signatures for non-intrusive load monitoring, IEEE Transactions on Smart Grid 5 (2) (2014) 870–878. doi:10.1109/TSG.2013.2271282.

[21] Y. H. Lin, M. S. Tsai, Non-intrusive load monitoring by novel neuro-fuzzy classification considering uncertainties, IEEE Transactions on Smart Grid 5 (5) (2014) 2376–2384. doi:10.1109/TSG.2014.2314738.

[22] S. Welikala, C. Dinesh, M. P. B. Ekanayake, R. I. Godaliyadda, J. Ekanayake, A real-time non intrusive load monitoring system, in: IEEE 11th International Conference on Industrial and Information Systems (ICIIS 2016), Roorkee, India, 2016.

[23] S. Welikala, C. Dinesh, R. I. Godaliyadda, M. P. B. Ekanayake, J. Ekanayake, Robust non-intrusive load monitoring (nilm) with unknown loads, in: 2016 IEEE International Conference on Information and Automation for Sustainability (ICIAfS), 2016, pp. 1–6. doi:10.1109/ICIAFS.2016.7946569.

[24] Y. H. Lin, M. S. Tsai, Development of an improved time - frequency analysis-based nonintrusive load monitor for load demand identification, IEEE Transactions on Instrumentation and Measurement 63 (6) (2014) 1470–1483. doi:10.1109/TIM.2013.2289700.

[25] S. Chen, Q. Chen, Y. Xu, Strategic bidding and compensation mechanism for a load aggregator with direct thermostat control capabilities, IEEE Transactions on Smart Grid PP (99) (2016) 1–1. doi:10.1109/TSG.2016.2611611.

[26] T. Hong, M. Lee, C. Koo, K. Jeong, J. Kim, Development of a method for estimating the rooftop solar photovoltaic (pv) potential by analyzing the available rooftop area using hillshade analysis, Applied Energy (2016) –doi:http://dx.doi.org/10.1016/j.apenergy.2016.07.001.
URL http://www.sciencedirect.com/science/article/pii/S0306261916309424

[27] S. Roy, Statistical estimates of short duration power generated by a photovoltaic unit in environment of scattered cloud cover, Energy 89 (2015) 14 – 23. doi:http://dx.doi.org/10.1016/j.energy.2015.06.038.
URL http://www.sciencedirect.com/science/article/pii/S036054421500794X

[28] G. Lorenzi, C. A. S. Silva, Comparing demand response and battery storage to optimize self-consumption in {PV} systems, Applied Energy 180 (2016) 524 – 535. doi:http://dx.doi.org/10.1016/j.apenergy.2016.07.103.
URL http://www.sciencedirect.com/science/article/pii/S030626191631042X

[29] H. Shaker, H. Zareipour, D. Wood, A data-driven approach for estimating the power generation of invisible solar sites, IEEE Transactions on Smart Grid 7 (5) (2016) 2466–2476. doi:10.1109/TSG.2015.2502140.

[30] H. Shaker, H. Zareipour, D. Wood, Estimating power generation of invisible solar sites using publicly available data, IEEE Transactions on Smart Grid 7 (5) (2016) 2456–2465. doi:10.1109/TSG.2016.2533164.

[31] B. O. Kang, K.-S. Tam, New and improved methods to estimate day-ahead quantity and quality of solar irradiance, Applied Energy 137 (2015) 240 – 249. doi:http://dx.doi.org/10.1016/j.apenergy.2014.10.021.
URL http://www.sciencedirect.com/science/article/pii/S0306261914010629

[32] B. M. Weedy, B. J. Cory, N. Jenkins, J. Ekanayake, G. Strbac, Electric power systems (2012).

[33] G. Morales-Espaa, L. Ramrez-Elizondo, B. F. Hobbs, Hidden power system inflexibilities imposed by traditional unit commitment formulations, Applied Energy 191 (2017) 223 – 238. doi:http://dx.doi.org/10.1016/j.apenergy.2017.01.089.
URL http://www.sciencedirect.com/science/article/pii/S0306261917301009

[34] M. Mazidi, H. Monsef, P. Siano, Robust day-ahead scheduling of smart distribution networks considering demand response programs, Applied Energy 178 (2016) 929 – 942. doi:http://dx.doi.org/10.1016/j.apenergy.2016.06.016.
URL http://www.sciencedirect.com/science/article/pii/S0306261916307917

[35] J. Ekanayake, N. Jenkins, K. Liyanage, J. Wu, A. Yokoyama, Smart grid: technology and applications (2012).

[36] Y. Zhang, W. Chen, R. Xu, J. Black, A cluster-based method for calculating baselines for residential loads, IEEE Transactions on Smart Grid 7 (5) (2016) 2368–2377. doi:10.1109/TSG.2015.2463755.

[37] H. G. C. P. Dinesh, D. B. W. Nettasinghe, G. M. R. I. Godaliyadda, M. P. B. Ekanayake, J. V. Wijayakulasooriya, J. B. Ekanayake, A subspace signature based approach for residential appliances identification using less informative and low resolution smart meter data, in: 2014 9th International Conference on Industrial and Information Systems (ICIIS), 2014, pp. 1–6. doi:10.1109/ICIINFS.2014.7036579.

[38] H. G. C. P. Dinesh, P. H. Perera, G. M. R. I. Godaliyadda, M. P. B. Ekanayake, J. B. Ekanayake, Residential appliance monitoring based on low frequency smart meter measurements, in: 2015 IEEE International Conference on Smart Grid Communications (SmartGridComm), 2015, pp. 878–884. doi:10.1109/SmartGridComm.2015.7436412.

[39] M. J. A. Ng, Y. Weiss, On spectral clustering: Analysis and an algorithm, MIT Press, Cambridge, 2002.

[40] L. L. et al., Estimation of total cloud cover from solar radiation observations at lake rotorua, new zealand, Elsevier Journal of Solar Energy 84(3) (2013) 501–506.

[41] E. Georges, B. Cornlusse, D. Ernst, V. Lemort, S. Mathieu, Residential heat pump as flexible load for direct control service with parametrized duration and rebound effect, Applied Energy 187 (2017) 140 – 153. doi:http://dx.doi.org/10.1016/j.apenergy.2016.11.012.
URL http://www.sciencedirect.com/science/article/pii/S0306261916315975

[42] G. Tsagarakis, R. C. Thomson, A. J. Collin, G. P. Harrison, A. E. Kiprakis, S. McLaughlin, Assessment of the cost and environmental impact of residential demand-side management, IEEE Transactions on Industry Applications 52 (3) (2016) 2486–2495. doi:10.1109/TIA.2016.2516478.

[43] I. Slimani, I. E. Farissi, S. A. Al-Qualsadi, Configuration of daily demand predicting system based on neural networks, in: 2016 3rd International Conference on Logistics Operations Management (GOL), 2016, pp. 1–5. doi:10.1109/GOL.2016.7731709.

[44] W. Elmenreich, Sensor fusion in time-triggered systems, Ph.D. thesis, Technische Universität Wien, Institut für Technische Informatik, Treitlstr. 3/3/182-1, 1040 Vienna, Austria (2002).

[45] N. Sharma, P. Sharma, D. Irwin, P. Shenoy, Predicting solar generation from weather forecasts using machine learning, in: Smart Grid Communications (SmartGridComm), 2011 IEEE International Conference on, 2011, pp. 528–533. doi:10.1109/SmartGridComm.2011.6102379.

[46] T. T. Teo, T. Logenthiran, W. L. Woo, Forecasting of photovoltaic power using extreme learning machine, in: Smart Grid Technologies - Asia (ISGT ASIA), 2015 IEEE Innovative, 2015, pp. 1–6. doi:10.1109/ISGT-Asia.2015.7387113.

[47] J. Kolter, M. Johnson, Redd: A public data set for energy disaggregation research, in: in Workshop on Data Mining Applications in Sustainability (SIGKDD), San Diego, CA, 2011.

[48] A. Reinhardt, et al., On the accuracy of appliance identification based on distributed load metering data, in: Proc. IEEE Int. Conf. Sustainable Internet and ICT for Sustainability(SustainlT'2012), 2012.

[49] D. L. Olson, D. Delen, Advanced Data Mining Techniques, 1st Edition, Springer Publishing Company, Incorporated, 2008.

[50] J. W. Taylor, Short-term load forecasting with exponentially weighted methods, IEEE Transactions on Power Systems 27 (1) (2012) 458–464. doi:10.1109/TPWRS.2011.2161780.

[51] N. Batra, et al., Nilmtk: An open source toolkit for non-intrusive load monitoring, in: Proceedings of the 5th International Conference on Future

Energy Systems, e-Energy '14, ACM, New York, NY, USA, 2014, pp. 265–276. doi:10.1145/2602044.2602051.
URL http://doi.acm.org/10.1145/2602044.2602051

[52] V. Stankovic, J. Liao, L. Stankovic, A graph-based signal processing approach for low-rate energy disaggregation, in: 2014 IEEE Symposium on Computational Intelligence for Engineering Solutions (CIES), 2014, pp. 81–87. doi:10.1109/CIES.2014.7011835.

[53] J. Z. Kolter, T. Jaakkola, Approximate inference in additive factorial hmms with application to energy disaggregation, in: Proc. 2012 Int. Conf. Artificial Intelligence and Statistics, 2012, pp. 1472–1482.

[54] J. Liao, G. Elafoudi, L. Stankovic, V. Stankovic, Power disaggregation for low-sampling rate data, in: 2nd International Non-intrusive Appliance Load Monitoring Workshop, Austin, TX, 2014.

[55] S. M. Tabatabaei, S. Dick, W. Xu, Toward non-intrusive load monitoring via multi-label classification, IEEE Transactions on Smart Grid 8 (1) (2017) 26–40. doi:10.1109/TSG.2016.2584581.

[56] S. Singh, A. Majumdar, Deep sparse coding for non-intrusive load monitoring, IEEE Transactions on Smart Grid PP (99) (2017) 1–1. doi:10.1109/TSG.2017.2666220.

[57] E. Elhamifar, S. Sastry, Energy disaggregation via learning 'powerlets' and sparse coding, in: Proceedings of the Twenty-Ninth AAAI Conference on Artificial Intelligence, AAAI'15, AAAI Press, 2015, pp. 629–635.
URL http://dl.acm.org/citation.cfm?id=2887007.2887095

[58] K. Basu, V. Debusschere, S. Bacha, U. Maulik, S. Bondyopadhyay, Non intrusive load monitoring: A temporal multi-label classification approach, IEEE Trans. Industrial Informatics 11 (4) (2015) 689–698.

[59] M. J. Johnson, A. S. Willsky, Bayesian nonparametric hidden semi-markov models, J. Mach. Learn. Res. 14 (1) (2013) 673–701.
URL http://dl.acm.org/citation.cfm?id=2502581.2502602

[60] B. Zhao, L. Stankovic, V. Stankovic, On a training-less solution for non-intrusive appliance load monitoring using graph signal processing, IEEE Access 4 (2016) 1784–1799. doi:10.1109/ACCESS.2016.2557460.

[61] M. Rana, I. Koprinska, A. Troncoso, Forecasting hourly electricity load profile using neural networks, in: 2014 International Joint Conference on Neural Networks (IJCNN), 2014, pp. 824–831. doi:10.1109/IJCNN.2014.6889489.